Top-Down Mass Spectrometry for Sequencing of Larger (up to 61 nt) RNA by CAD and EDD

Monika Taucher and Kathrin Breuker

Institute of Organic Chemistry and Center for Molecular Biosciences (CMBI), University of Innsbruck, Innsbruck, Austria

We have studied the effect of solution additives on hydrolysis and charge state distribution in ESI MS of RNA. Lower and higher charge state ions can be electrosprayed from solutions containing 25 mM piperidine/25 mM imidazole and 1% vol. triethylamine, respectively, with base-catalyzed hydrolysis rates that are sufficiently slow to perform MS/MS experiments. These lower and higher charge state ions are suitable as precursors for CAD and EDD, respectively. We demonstrate nearly complete sequence coverage for 61 nt RNA dissociated by CAD, and 34 nt RNA dissociated by EDD, and suggest a mechanism for backbone fragmentation in EDD of RNA. (J Am Soc Mass Spectrom 2010, 21, 918–929) © 2010 American Society for Mass Spectrometry

The "top-down" approach is increasingly being applied in mass spectrometry (MS) studies of proteins [1–5], using mostly collisionally activated dissociation (CAD) [6–8], electron capture dissociation (ECD) [9–12], or electron-transfer dissociation (ETD) [13] for generation of sequence-informative fragment ions from backbone cleavage in multiply protonated precursor ions. First examples of top-down mass spectrometry of smaller (up to 25 nt) multiply deprotonated desoxyribonucleic acids (DNA) were reported in the early 1990s [14–16], and the concept was soon extended to larger (up to 108 nt) DNA [17].

For ribonucleic acids (RNAs), the development and application of mass spectrometry-based methodology has been much slower than for DNA [18], possibly because the significance of RNA in regulation of gene expression was recognized only recently [19]. Top-down MS has been applied to study RNA modified by structural probes [20], for characterization of conserved domains of the HIV-1 packaging signal RNA [21], for investigating aptamer/ligand complexes [22], and binding of antibiotics to ribosomal RNA subdomains [23]. However, sequencing by top-down mass spectrometry of RNA $>$ 20 nt has been demonstrated only recently, as discussed below.

Collisionally activated dissociation of multiply deprotonated RNA from electrospray ionization (ESI) [24] has lately provided full sequence coverage for small interfering RNA (siRNA) [25] and a riboswitch aptamer domain sequence [26] consisting of 21 and 34 nucleotides (nt), respectively. Mass spectral quality, particularly with regard to undesired secondary fragmentation, was shown to critically depend on precursor ion charge [25, 27] and collisional cooling of primary fragments [26]. Our rationale for the decrease in secondary fragmentation was that reduced net charge and collisional cooling minimize the internal energy of fragment ions from primary backbone cleavage, which makes them less prone to secondary fragmentation [26]. In our study of 34 nt RNA, we used ions of relatively low net charge, $(M - 7H)^{7-}$, which were electrosprayed from acidified solutions [26].

However, mass spectrometer performance generally decreases with increasing mass-to-charge ratio, i.e., lower ion charge. An alternative method that was reported to actually give higher yields of sequence-informative fragment ions from more highly and negatively charged precursors [28, 29] is electron detachment dissociation (EDD), which was introduced by Zubarev and coworkers as a new technique for dissociation of peptide anions [30]. In EDD, bombardment of multiply deprotonated peptides [31–33], oligonucleotides [29, 34–38], or oligosaccharides [28, 39–43] with $>$10 eV electrons results in electron detachment, producing $(M - nH)^{(n-1)-\bullet}$ radical ions that can undergo backbone dissociation [37, 38]. To date, only one study on EDD of RNA (6 nt) has been published [44], with only one of the sequences (GCAUAC) allowing for unambiguous assignment of fragment ion identity (in 3′- and 5′-OH terminated homonucleotides, e.g., A_6, the following ions cannot be distinguished from each other based on their mass values: *a* from *z*, *b* from *y*, *c* from *x*, and *d* from *w*). Yang and Håkansson reported that the most abundant fragments in EDD of $(GCAUAC - 2H)^{2-}$ were *w* and *d* ions, but *c* and *y* ions were also observed [44]. We have studied here CAD and EDD of $(M - nH)^{n-}$ ions of larger (up to 61 nt) RNA, and propose a mechanism for backbone cleavage in EDD.

Address reprint requests to Dr. K. Breuker, Institute of Organic Chemistry and Center for Molecular Biosciences (CMBI), University of Innsbruck, Innrain 52a, A-6020 Innsbruck, Austria. E-mail: kathrin.breuker@uibk.ac.at

1044-0305/10/$32.00
doi:10.1016/j.jasms.2010.02.025

Published online March 9, 2010
Received November 23, 2009
Revised February 18, 2010
Accepted February 18, 2010

Experimental

RNA was prepared using a solid-phase synthesis approach described recently [45], followed by HPLC purification and desalting using vivaspin 500 centrifugal concentrators (Sartorius, Göttingen, Germany; PES membrane, MWCO 3000 or 5000), see reference [26] for details. The RNA sequences were 22 nt: GGACG AUACG CGUGA AGCGU CC, 34 nt (A): AGUCG UGCUA GCAAA ACCGG CUUUA AAAAA CUAG, 34nt (B): AGAUG UGCCG GCAAA ACCAU CUUUA AAAAA CCGG, 57 nt: AGUGG UUCGU AACCC UCCCA CUUGA ACAAC CAACA AUUGU UCGAA ACAAA ACUAG GA, and 61 nt: AGAUG UGCUA GCAAA ACCAU CUUUA AAAAA CUAGA CUUGG GGUGC AAGUC CCCUU UUUUA U, with hydroxyl groups at the 3′ and 5′ termini. The 34 nt sequence A carried OCH_3 groups at the ribose C2′-positions of C4 and A30, and the 61 nt sequence had a mass-silent base modification at position 33 (2-amino purine instead of 6-amino purine, which is adenine). RNA mass values were determined from ESI spectra with internal calibration (error ~1 ppm) using ion signals of polyethylene glycol that was added to the spray solution. Measured mass values (most abundant isotope peak) were 7095.0109 (22 nt, $m_{calculated}$ 7095.0176), 10,940.557 (34 nt, A, $m_{calculated}$ 10,940.567), 10,911.567 (34 nt, B, $m_{calculated}$ 10,911.551), 18,209.485 (57 nt, $m_{calculated}$ 18,209.518), 19468.532 (61 nt, $m_{calculated}$ 19468.561). Methanol (Acros, Vienna, Austria) was HPLC grade. Triethylamine (puriss p.a., ≥ 99.5%), acetic acid (puriss p.a., ≥ 99.8%), piperidine (puriss p.a., ≥ 99.0%), and imidazole (puriss p.a., ≥ 99.5%) were purchased from Sigma-Aldrich (Vienna, Austria).

MS and MS/MS experiments were performed on a 7 Tesla Fourier transform-ion cyclotron resonance (FT-ICR) mass spectrometer (Apex ultra 70; Bruker Austria GmbH, Vienna, Austria) equipped with an electrospray ionization (ESI) source and a hollow dispenser cathode for ECD/EDD experiments. Ions were transferred through two ion funnels into a linear hexapole trap for ion accumulation, an *m/z*-selective quadrupole, and a second linear hexapole trap floated with Argon for collisional activation or collisionally activated dissociation, see reference [26] for details. Laboratory frame collision energy is defined here as the bias potential difference between the second ion funnel and the collision cell hexapole times the ion's charge. Ion transfer and focusing into the ICR cell used electrostatic ion optical elements. ESI solutions were 1 μM RNA in 1:1 H_2O/CH_3OH, with 1% vol. triethylamine, 0.05% vol. acetic acid, or an equal mixture of piperidine and imidazole (final concentration 25 mM each) as additives. ESI flow rate was 1.5–2.0 μL/min. For increased statistics, MS/MS spectra were the sum of 500 scans, except for the EDD spectrum of 61 nt RNA which was the sum of 800 scans. Between 20 and 50 scans were added in 1.5 to 3.5 min, respectively, for monitoring RNA hydrolysis.

CAD Experiments

After precursor ion selection in the quadrupole, ions were accelerated into the collision cell for CAD and accumulated for 1 s. Collision energies were adjusted to give ~75% fragmentation. Collision gas flow rate was >0.2 l/s to promote collisional cooling of primary fragment ions. Addition of piperidine and imidazole to the ESI solution (final concentration 25 mM each) required increased funnel-skimmer voltages (about −90 V compared with −30 to 0 V for the other additives) for efficient dissociation of RNA/piperidine clusters (Figure S1, which can be found in the electronic version of this article). CAD mass spectra were calibrated by single point correction (mass error ~10 ppm) of the external calibration function using the calculated *m/z* value of the most abundant isotope of the precursor ion $(M - nH)^{n-}$.

EDD Experiments

For EDD experiments, precursor ions were first selected in the quadrupole, accumulated in the linear hexapole collision cell for 0.1 s, and transferred into the ICR cell, where a radiofrequency waveform was applied as a second isolation event. This was necessary because collisional activation in the hexapole collision cell (up to 50 eV laboratory frame collision energy) resulted in formation of some *c*- and *y*-fragments. Collision gas flow rate was <0.2 l/s to minimize deactivation of precursor ions in the collision cell. Electrons emitted from the indirectly heated hollow dispenser cathode (heating current 1.6 A) were pulsed into the ICR cell for 0.15–0.8 s, with electron energies of 18 or 24 eV. EDD mass spectra were calibrated internally (mass error ~ 1 ppm) using calculated *m/z* values of the most abundant isotopes of $(M - nH)^{n-}$, $(M - nH)^{(n-1)-\bullet}$, $(M - nH)^{(n-2)-\bullet\bullet}$, $(M - 10H)^{(n-3)-\bullet\bullet\bullet}$, etc. ions with a calibration function with a linear and a quadratic term.

Results and Discussion

CAD Experiments

As discussed in the introduction, CAD of multiply deprotonated RNA can produce MS/MS spectra suitable for de novo sequencing, given that the precursor ions carry a relatively low negative net charge (about −0.2/nt) and that the fragment ions from primary backbone dissociation are deactivated by collisional cooling. In our recent study [26], we obtained complete sequence coverage from terminal fragments in CAD of $(M - 7H)^{7-}$ ions of 34 nt RNA, and 30 out of 32 possible complementary ion pairs. For lowering the precursor ion charge down to −7, we used acetic acid; acid-catalyzed hydrolysis of 34 nt RNA upon addition of 0.05% vol. acetic acid was sufficiently slow to perform CAD MS experiments within ~1 h after preparation of

the ESI solution [26]. However, for larger RNA (57 nt and 61 nt), we find that acid-catalyzed hydrolysis proceeds at a too high rate to obtain CAD spectra, or monitor the kinetics of hydrolysis by mass spectrometry. Presumably the larger number of backbone sites that can potentially undergo hydrolysis accounts for faster degradation of 57 and 61 nt RNA.

Greig and Griffey reported that DNA electrosprayed from 25 mM piperidine/25 mM imidazole solutions produced high ion yields in negative mode ESI MS, along with efficient suppression of sodium and potassium adduct ions [46]. Importantly, they also observed a reduction in average net charge of $(M - nH)^{n-}$ ions upon addition of piperidine/imidazole. We have monitored by mass spectrometry the effect of adding acetic acid, triethylamine, and piperidine/imidazole on the charge state distribution and hydrolysis of 34 nt RNA (Figure 1). ESI MS spectra recorded one hour after preparation of the solutions are shown in Figure 1a–c; although acetic acid is most effective in lowering negative net charge of RNA, molecular ion abundance is significantly reduced by hydrolysis (Figure 1a). In contrast, addition of triethylamine (Figure 1b) or piperidine/imidazole (Figure 1c) gives abundant molecular ions and negligible products from hydrolysis, with the latter additive yielding molecular ions of relatively low charge (around −9). Reference spectra without additive obtained by electrospraying 34 nt RNA (1 μM) from 1:1 methanol/water solutions showed no discernible RNA ion signals, possibly because of extensive salt adduction.

While acid-catalyzed hydrolysis (0.05% vol. acetic acid, pH 2.5) of the 34 nt RNA is complete after 5 h (Figure 1d), base-catalyzed hydrolysis (triethylamine, pH 9.5, and piperidine/imidazole, pH 11.5) proceeds at a smaller rate (~0.1/h compared with ~0.4/h for acetic acid). RNA deprotonation in solution is more efficient at pH 11.5 (25 mM piperidine/25 mM imidazole) than at pH 9.5 (1% vol. triethylamine), but the Figure 1 spectra show higher negative net charge for ions electrosprayed from solutions with triethylamine added. This demonstrates that factors other than solution pH, such as surface tension of the ESI droplets [47] and gas-phase ion chemistry during and after the ESI process [48] play an important role in determining the final net charge of RNA ions. In ESI spectra of 34 nt RNA with piperidine/imidazole as additive, we observe piperidine adducts to molecular ions; employing a higher skimmer potential (about −90 V) effects dissociation of the adducts and further lowers the average molecular ion charge (Figure S1). This observation suggests that piperidine dissociates in the gas phase from RNA anions in its deprotonated form, leaving the labile amine proton on the multiply deprotonated RNA and thereby lowering RNA net charge.

We next used piperidine/imidazole as additives to ESI solutions of 57 and 61 nt RNA at −90 V skimmer potential, which produces abundant molecular ions of

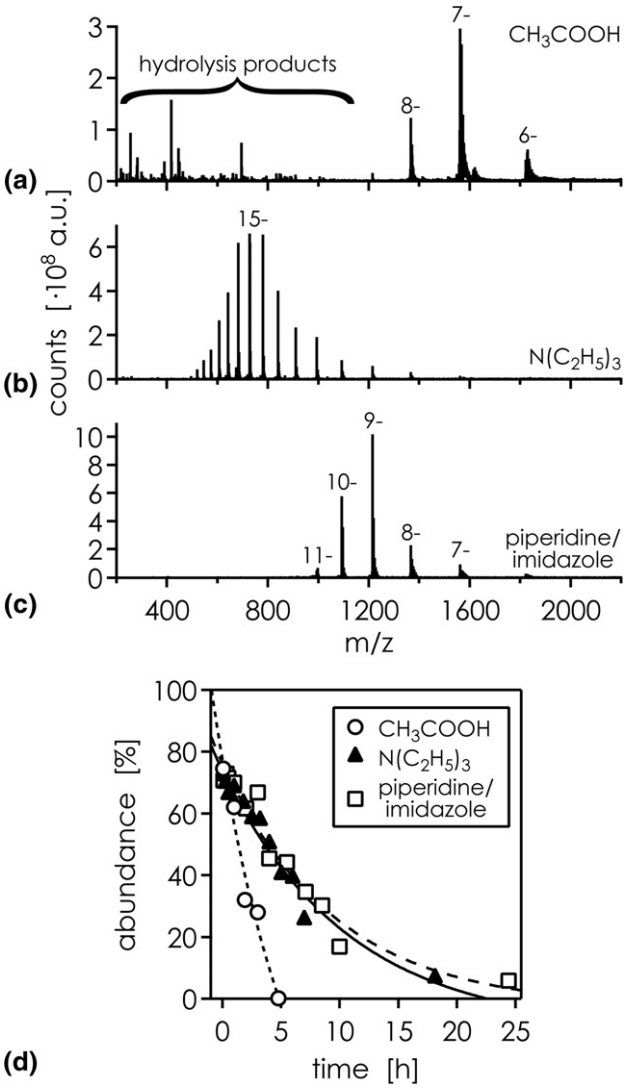

Figure 1. MS spectra of 34 nt RNA (sequence A) obtained 1 h after preparation of ESI solutions (1 μM in 1:1 H_2O/CH_3OH) with (**a**) 0.05% vol. acetic acid (pH 2.5), skimmer potential 0 V, 50 scans added; (**b**) 1% vol. triethylamine (pH 9.5), skimmer potential 0 V, 40 scans added; (**c**) 25 mM piperidine/25 mM imidazole (pH 11.5), skimmer potential −90 V, 20 scans added; (**d**) relative molecular ion abundance versus time after preparation of ESI solution; values at ~0 h are not 100% because of chemical noise in the spectra.

relatively low negative net charge (*m/z* 1000–1600, Figure S2); the molecular ion signals are stable for at least 3 h. CAD of $(M - 12H)^{12-}$ ions of 57 nt RNA gives nearly complete sequence coverage from *c*, *y*, and *w* fragment ions, and shows little dependence of fragment ion yield on nucleobase sequence (Figure S2).

Similar results are obtained for CAD of 61 nt RNA. In the CAD spectrum of $(M - 13H)^{13-}$ ions of 61 nt RNA (*m/z* 1500) shown in Figure 2a, 98% of all assigned fragment ions are from backbone cleavage via the *c/y* channel; only 2% are from the *a/w* channel. Out of the *c* ions, 5% show base loss, whereas base loss from *a*, *w*, and *y* ions is 100%, 5%, and 1%, respectively. Sequence

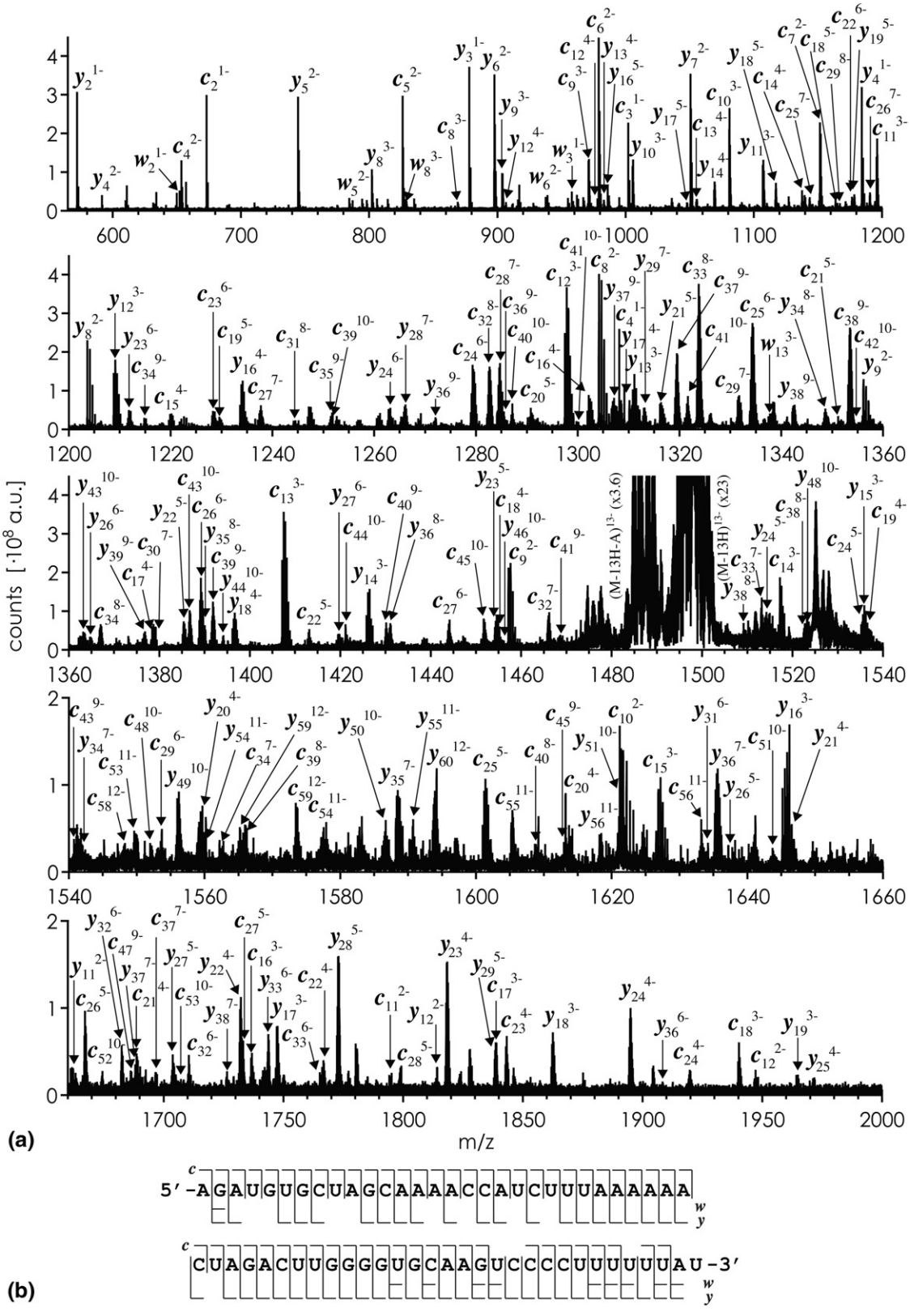

Figure 2. (**a**) CAD spectrum (laboratory-frame collision energy 182 eV) of $(M - 13H)^{13-}$ ions from ESI of 61 nt RNA (1 μM in H_2O/CH_3OH 1:1, 25 mM piperidine/25 mM imidazole, pH 11.5); (**b**) fragment ion map illustrating sequence coverage.

coverage from the c/y channel is nearly complete (Figure 2b), with only y_1 missing (y_1 lacks a phosphate as deprotonation site and cannot be detected). Importantly for de novo sequencing, we obtain 47 out of 59 (80%) possible complementary c/y ion pairs.

This extension of top-down MS to >60 nt RNA almost doubles the size of RNA for which virtually complete sequence information can be obtained from a single CAD spectrum [26], and is a major step towards de novo sequencing of even larger RNA. However, it would be worthwhile to study alternative dissociation methods involving more highly charged precursor ions, as instrument performance generally goes down with decreasing ion charge. In particular, sensitivity and mass resolving power decrease linearly with decreasing ion charge in FT-ICR MS [49]. This consideration led us to turn our attention to EDD of multiply deprotonated RNA.

EDD Experiments

Figure 3 shows an EDD spectrum of $(M - 10H)^{10-}$ ions of 22 nt RNA obtained with 18 eV electron energy. The gas-phase structures of the $(M - 10H)^{10-}$ RNA ions (0.45 charges/nt) are not known, but ion mobility studies showed that larger oligonucleotides (28 nt, 40 nt, 55 nt) carrying >0.35 negative charges per nucleotide generally have extended conformations [50]. Moreover, the $(M - 10H)^{10-}$ RNA ions here were heated by energetic collisions (50 eV laboratory frame collision energy) in the linear hexapole collision cell to prevent formation of higher order gas-phase structure; after trapping and before bombardment with electrons in the ICR cell, the ions were again isolated by application of a radiofrequency waveform. Nevertheless, the yield of backbone fragments is relatively small; only 25% of all EDD products are from RNA backbone cleavage. We observe exclusively even-electron d and w-type fragments (Figure 3, Table 1), but no radical backbone fragments as could be expected for unimolecular dissociation of the radical $(M - 10H)^{9-\bullet}$ ions formed by electron detachment. Only in experiments without isolation of the $(M - 10H)^{10-}$ ions in the ICR cell, even-electron c and y-type ions of relatively low abundance (15% compared with 85% d and w-type ions) were observed, with the average charges of complementary c_i and $y_{(22-i)}$ ions adding up to 10–. This demonstrates that c and y-type ions are not products from electron detachment dissociation, but merely adventitious fragment ions from energetic activation. The d and w-type ions are noncomplementary; mass values of d_i and $w_{(22-i)}$ fragments add up to mass values that are 97.98 Da (H_3PO_4) higher than that of the 22 nt RNA. Oxidized molecular ions from electron detachment (i.e., $(M - 10H)^{9-\bullet}$, $(M - 10H)^{8-\bullet\bullet}$, $(M - 10H)^{7-\bullet\bullet\bullet}$, and $(M - 10H)^{6-\bullet\bullet\bullet\bullet}$) make up 67% of all EDD products. Other products (8%) include loss of adenine (3.5%) and uracil (0.5%) from oxidized molecular ions, as well as yet unassigned fragments (4.5%) with mass values 167.03 Da lower than those of the oxidized molecular ions.

The yield of d and w fragment ions versus cleavage site is shown in Figure 4a, along with nucleobase ionization energies (IEs) [51]. The yield of d ions (black bars) is generally higher on the 3′-side of nucleobases with lower IEs (A: 8.3 ± 0.1 eV, G: 8.0 ± 0.1 eV) [51], and negligibly small on the 3′-side of nucleobases with higher IEs (C: 9.0 ± 0.1 eV, U: 9.4 ± 0.1 eV) [51]. In contrast, w ion yields (gray bars) generally appear to peak on the 5′-side of nucleobases with lower IE, and are lower on the 5′-side of nucleobases with higher IE. In the A6–G14 region where nucleobases with lower and higher IEs alternate, d and w ion yields also alternate. Moreover, d and w yields are highest in the A/G-rich regions at the 5′ terminus (G1–A3) and towards the 3′ terminus (G14–G19). These findings clearly show that there is a strong correlation of both d and w fragment ion yield with nucleobase ionization energy, and suggest that backbone dissociation in EDD

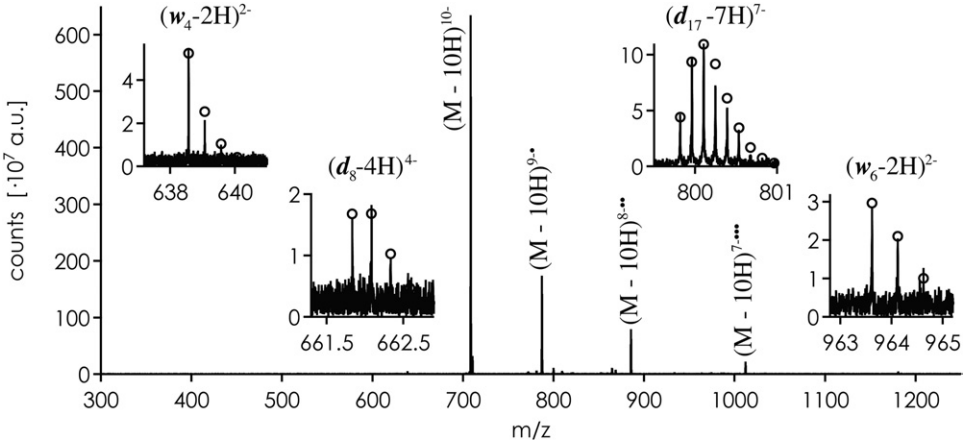

Figure 3. EDD (electron energy 18 eV) spectrum of $(M - 10H)^{10-}$ ions from ESI of 22 nt RNA (1 μM in H_2O/CH_3OH 1:1, 1% vol. Et_3N, pH 9.5); insets show signals of characteristic fragment ions from backbone cleavage and their calculated isotopic distributions (circles).

Table 1. For the EDD spectrum in Figure 3, measured and calculated *m/z* values of fragment ions from backbone cleavage, elemental ion compositions, and mass errors (calculated *m/z* – measured *m/z*, in ppm); *most abundant isotopic peak (4) used for internal calibration; all other mass values are for monoisotopic peaks

Measured *m/z*	Assignment	Calculated *m/z*	Elemental ion composition	Error [ppm]
708.49448*	$(M - 10H)^{10-}$	708.49448	$(C_{211}H_{262}N_{89}O_{150}P_{21} - 10H)^{10-}$	0.00
787.21603*	$(M - 10H)^{9-\bullet}$	787.21603	$(C_{211}H_{262}N_{89}O_{150}P_{21} - 10H - e)^{9-\bullet}$	0.00
885.61807*	$(M - 10H)^{8-\bullet\bullet}$	885.61797	$(C_{211}H_{262}N_{89}O_{150}P_{21} - 10H - 2e)^{8-\bullet\bullet}$	−0.11
1012.13458*	$(M - 10H)^{-\bullet\bullet\bullet}$	1012.13475	$(C_{211}H_{262}N_{89}O_{150}P_{21} - 10H - 3e)^{7-\bullet\bullet\bullet}$	0.17
1180.82386*	$(M - 10H)^{6-\bullet\bullet\bullet\bullet}$	1180.82378	$(C_{211}H_{262}N_{89}O_{150}P_{21} - 10H - 4e)^{6-\bullet\bullet\bullet\bullet}$	−0.07
322.04435	$(w_1 - H)^-$	322.04457	$(C_9H_{14}N_3O_8P_1 - H)^-$	0.68
362.05054	$(d_1 - H)^-$	362.05072	$(C_{10}H_{14}N_5O_8P_1 - H)^-$	0.50
627.08557	$(w_2 - H)^-$	627.08586	$(C_{18}H_{26}N_6O_{15}P_2 - H)^-$	0.46
466.05183	$(w_3 - 2H)^{2-}$	466.05194	$(C_{27}H_{37}N_8O_{23}P_3 - 2H)^{2-}$	0.24
517.57142	$(d_3 - 2H)^{2-}$	517.57170	$(C_{30}H_{38}N_{15}O_{21}P_3 - 2H)^{2-}$	0.54
638.57578	$(w_4 - 2H)^{2-}$	638.57566	$(C_{37}H_{49}N_{13}O_{30}P_4 - 2H)^{2-}$	−0.19
527.06182	$(w_5 - 3H)^{3-}$	527.06178	$(C_{46}H_{61}N_{16}O_{37}P_5 - 3H)^{3-}$	−0.08
791.09485	$(w_5 - 2H)^{2-}$	791.09631	$(C_{46}H_{61}N_{16}O_{37}P_5 - 2H)^{2-}$	1.85
561.40793	$(d_5 - 3H)^{3-}$	561.40828	$(C_{49}H_{62}N_{23}O_{35}P_5 - 3H)^{3-}$	0.63
642.07771	$(w_6 - 3H)^{3-}$	642.07759	$(C_{56}H_{73}N_{21}O_{44}P_6 - 3H)^{3-}$	−0.19
963.62034	$(w_6 - 2H)^{2-}$	963.62002	$(C_{56}H_{73}N_{21}O_{44}P_6 - 2H)^{2-}$	−0.33
671.09223	$(d_6 - 3H)^{3-}$	671.09246	$(C_{59}H_{74}N_{28}O_{41}P_6 - 3H)^{3-}$	0.34
751.76061	$(w_7 - 3H)^{3-}$	751.76176	$(C_{66}H_{85}N_{26}O_{50}P_7 - 3H)^{3-}$	1.53
661.83588	$(d_8 - 4H)^{4-}$	661.83698	$(C_{78}H_{97}N_{35}O_{55}P_8 - 4H)^{4-}$	1.66
732.09386	$(w_9 - 4H)^{4-}$	732.09449	$(C_{86}H_{109}N_{36}O_{63}P_9 - 4H)^{4-}$	0.86
824.34845	$(d_{10} - 4H)^{4-}$	824.35916	$(C_{97}H_{121}N_{43}O_{69}P_{10} - 4H)^{4-}$	0.17
715.68735	$(w_{11} - 5H)^{5-}$	715.68869	$(C_{105}H_{132}N_{43}O_{78}P_{11} - 5H)^{5-}$	1.87
789.30330	$(d_{12} - 5H)^{5-}$	789.30362	$(C_{116}H_{145}N_{51}O_{83}P_{12} - 5H)^{5-}$	0.40
845.70749	$(w_{13} - 5H)^{5-}$	845.70643	$(C_{124}H_{156}N_{51}O_{92}P_{13} - 5H)^{5-}$	−1.25
755.42827	$(w_{14} - 6H)^{6-}$	755.42769	$(C_{133}H_{168}N_{54}O_{99}P_{14} - 6H)^{6-}$	−0.76
766.09720	$(d_{14} - 6H)^{6-}$	766.09726	$(C_{135}H_{168}N_{58}O_{98}P_{14} - 6H)^{6-}$	0.07
810.26917	$(w_{15} - 6H)^{6-}$	810.26978	$(C_{143}H_{180}N_{59}O_{105}P_{15} - 6H)^{6-}$	0.75
703.51889	$(d_{15} - 7H)^{7-}$	703.51840	$(C_{145}H_{180}N_{63}O_{104}P_{15} - 7H)^{7-}$	−0.70
820.93958	$(d_{15} - 6H)^{6-}$	820.93934	$(C_{145}H_{180}N_{63}O_{104}P_{15} - 6H)^{6-}$	−0.29
985.32916	$(d_{15} - 5H)^{5-}$	985.32867	$(C_{145}H_{180}N_{63}O_{104}P_{15} - 5H)^{5-}$	−0.50
861.27215	$(w_{16} - 6H)^{6-}$	861.27310	$(C_{152}H_{191}N_{61}O_{113}P_{16} - 6H)^{6-}$	2.15
875.78138	$(d_{16} - 6H)^{6-}$	875.78143	$(C_{155}H_{192}N_{68}O_{110}P_{16} - 6H)^{6-}$	0.06
1051.13810	$(d_{16} - 5H)^{5-}$	1051.13917	$(C_{155}H_{192}N_{68}O_{110}P_{16} - 5H)^{5-}$	1.02
799.81821	$(d_{17} - 7H)^{7-}$	799.81839	$(C_{165}H_{204}N_{73}O_{117}P_{17} - 7H)^{7-}$	0.23
933.28920	$(d_{17} - 6H)^{6-}$	933.28934	$(C_{165}H_{204}N_{73}O_{117}P_{17} - 6H)^{6-}$	0.15
834.39064	$(w_{18} - 7H)^{7-}$	834.39095	$(C_{172}H_{215}N_{71}O_{126}P_{18} - 7H)^{7-}$	0.37
984.13022	$(d_{18} - 6H)^{6-}$	984.12955	$(C_{174}H_{216}N_{76}O_{124}P_{18} - 6H)^{6-}$	−0.68
768.09612	$(w_{19} - 8H)^{8-}$	768.09633	$(C_{181}H_{227}N_{74}O_{133}P_{19} - 8H)^{8-}$	0.28
780.97628	$(d_{19} - 8H)^{8-}$	780.97627	$(C_{184}H_{228}N_{81}O_{131}P_{19} - 8H)^{8-}$	−0.01
892.68739	$(d_{19} - 7H)^{7-}$	892.68821	$(C_{184}H_{228}N_{81}O_{131}P_{19} - 7H)^{7-}$	0.92
809.22792	$(w_{20} - 8H)^{8-}$	809.22790	$(C_{191}H_{239}N_{79}O_{139}P_{20} - 8H)^{8-}$	−0.03
819.22883	$(d_{20} - 8H)^{8-}$	819.22944	$(C_{193}H_{239}N_{83}O_{139}P_{20} - 8H)^{8-}$	0.74
852.35889	$(w_{21} - 8H)^{8-}$	852.35883	$(C_{201}H_{251}N_{84}O_{146}P_{21} - 8H)^{8-}$	−0.08
974.26624	$(w_{21} - 7H)^{7-}$	974.26827	$(C_{201}H_{251}N_{84}O_{146}P_{21} - 7H)^{7-}$	2.09

of RNA is initiated by electron detachment from the nucleobases. Under the reasonable assumption that backbone cleavage next to nucleobases with lower IE is more efficient than backbone cleavage next to nucleobases with higher IE, the yield of d_i ions is generally affected by nucleobase i, whereas the yield of w_i ions is generally affected by nucleobase $(22 - i - 1)$ (Table 2). For example, *d* ion yields are highest for d_{15} and d_{17}, and *w* ion yields are highest for w_4 $(22 - 17 - 1 = 4)$ and w_6 $(22 - 15 - 1 = 6)$.

To quantify the effect of nucleobase IE on backbone fragmentation, Figure 4b displays added yields of *d* and *w* fragments from cleavage affected by nucleobases A, C, G, and U, respectively, normalized to the number of bases involved (A: 5; C: 5; G: 8; U: 3 for *d* ions, and A: 5; C: 4; G: 8; U: 3 for *w* ions) versus nucleobase IE. This analysis reveals that ~87% of all backbone fragments are from cleavage affected by the purine bases A and G with lower IEs, and only ~13% are from cleavage affected by the pyrimidine bases C and U with higher IEs (Figure 4b). A recent EDD study of DNA found different electron detachment efficiencies for different hexameric homonucleotides, with $dG_6 > dT_6 > dA_6 > dC_6$ [37]. In contrast, electron detachment efficiencies in electron photodetachment dissociation (EPD) follow the trend $dG_6 > dA_6 > dC_6 > dT_6$ [52]. Our EDD data here agree qualitatively with the EPD data in that higher efficiency is found for the purine bases, but they dis-

agree with the above EDD data on DNA. Nevertheless, the DNA study and our RNA data clearly show that EDD of nucleic acids is affected by nucleobase IE.

Scheme 1 illustrates two reaction pathways consistent with the observation of noncomplementary even-electron d and w ions in EDD of RNA. As discussed above, nucleobase i of 22 nt RNA affects the yield of d_i and $w_{(22\text{-}i\text{-}1)}$ ions; for cleavage next to nucleobase G10 in Scheme 1 this corresponds to d_{10} and w_{11}. In one pathway, electron detachment from G10 gives radical ions $(M - nH)^{(n-1)-\bullet}$ that dissociate into complementary $a_{11}^{\bullet}/w_{11}$ ion pairs (Scheme 1, left). Facile loss of the radical nucleoside unit from $a_{11}^{\bullet}$ ions then gives d_{10} ions. In the other pathway, electron detachment gives complementary $d_{10}/z_{12}^{\bullet}$ ion pairs, and loss of the radical nucleoside unit from $z_{12}^{\bullet}$ ions gives w_{11} ions (Scheme 1, right). However, the pathway producing $a^{\bullet}/w$ ions (Scheme 1, left) is unlikely because not the first but the second 3′C-O ribose-phosphate bond

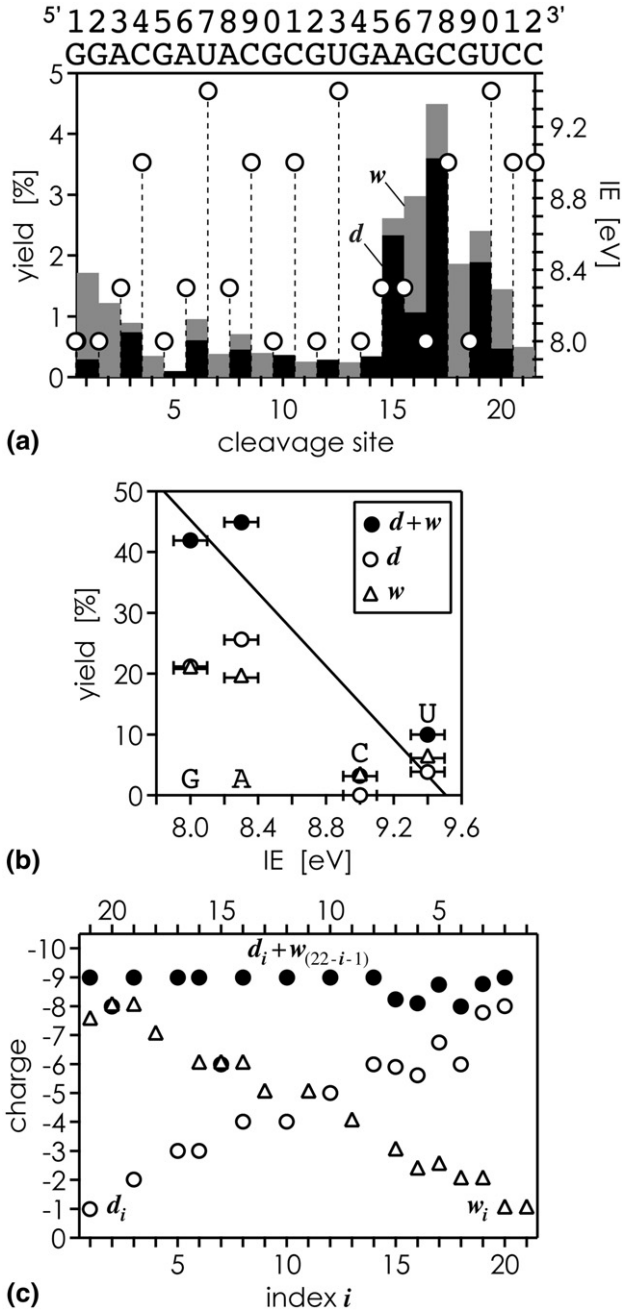

Figure 4. For the EDD spectrum in Figure 3, (**a**) d (black bars) and w (gray bars) ion yield (left axis) versus cleavage site between nucleotide units, and nucleobase ionization energies (IEs, open circles, right axis); (**b**) backbone fragment ion yield from cleavage affected by nucleobases A, G, C, and U, normalized to the number of bases involved, for d_i and $w_{(22\text{-}i\text{-}1)}$ ions affected by base i; (**c**) average net charge of d_i and w_i fragment ions versus i, with d_i (open circles) and w_i (triangles) data plotted versus the bottom and top axes, respectively; added average charge of d_i and $w_{(22\text{-}i\text{-}1)}$ ions (filled circles) plotted versus the bottom axis.

Table 2. For the EDD spectrum in Figure 3, site-specific d and w ion yields aligned such that nucleobases with lower IE (**bold**) correspond to higher yields and vice versa

5′-Fragment	Yield [%]	Nucleobase	IE [eV]	3′-Fragment	Yield [%]
				w_{21}	1.423
d_1	**0.293**	**G1**	**8**	w_{20}	**1.220**
d_2	**0**	**G2**	**8**	w_{19}	**0.149**
d_3	**0.741**	**A3**	**8.3**	w_{18}	**0.347**
d_4	0	C4	9	w_{17}	0
d_5	**0.098**	**G5**	**8**	w_{16}	**0.349**
d_6	**0.606**	**A6**	**8.3**	w_{15}	**0.383**
d_7	0	U7	9.4	w_{14}	0.253
d_8	**0.452**	**A8**	**8.3**	w_{13}	**0.397**
d_9	0	C9	9	w_{12}	0
d_{10}	**0.364**	**G10**	**8**	w_{11}	**0.253**
d_{11}	0	C11	9	w_{10}	0
d_{12}	**0.286**	**G12**	**8**	w_9	**0.241**
d_{13}	0	U13	9.4	w_8	0
d_{14}	**0.344**	**G14**	**8**	w_7	**0.278**
d_{15}	**2.334**	**A15**	**8.3**	w_6	**1.914**
d_{16}	**1.064**	**A16**	**8.3**	w_5	**0.894**
d_{17}	**3.600**	**G17**	**8**	w_4	**1.859**
d_{18}	0.004	C18	9	w_3	0.512
d_{19}	**1.892**	**G19**	**8**	w_2	**0.977**
d_{20}	0.468	U20	9.4	w_1	0.495
d_{21}	0	C21	9		
		C22	9		

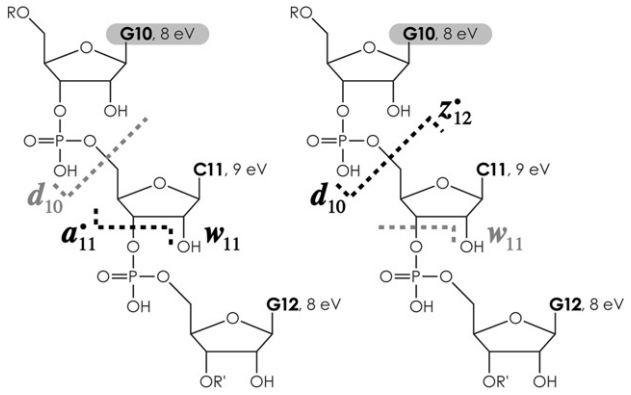

Scheme 1. Possible reaction pathways for the formation of d and w ions in EDD of RNA, illustrated here for electron detachment from G10 in 22 nt RNA.

away from the initial radical site would break in the first step.

Our data and above considerations strongly suggest a mechanism in which even-electron d_i ions are produced by primary backbone cleavage on the 3′ side of nucleobase i, along with radical complements $z_{(22\text{-}i)}$ that undergo rapid secondary fragmentation to form even-electron $w_{(22\text{-}i\text{-}1)}$ ions by loss of a radical nucleoside unit (Scheme 1, right). In further support of this hypothesis, the average charges of d_i and $w_{(22\text{-}i\text{-}1)}$ ions generally add up to the charge of the most abundant radical ions formed by electron detachment, $(M - 10H)^{9-\bullet}$ (Figure 4c).

A possible mechanism for backbone cleavage in EDD of RNA is shown in Scheme 2. Here, electron detachment from a nucleobase creates a positive charge that is neutralized by electron-transfer from the adjacent phosphate, along with hydrogen abstraction from the ribose (I–II). The newly formed radical site at the ribose C5′-position reacts with its nucleobase to form a cyclic intermediate (II–III). This type of reaction has been observed experimentally in DNA in vitro, and in human cells exposed to ionizing radiation ("tandem lesions" in DNA damage) [53–55]. Calculations suggest that the reaction is only marginally endoergic in the gas phase, with free energies between 3 and 10 kJ/mol [56]. Cleavage of the C5′-O phosphoester bond is initiated by proton abstraction from the ribose C4′-position (III–IV), and produces a pair of complementary d and $z^{\bullet}$ ions (IV). According to Bredt's rule, formation of the double-bond between C4′ and C5′ is energetically costly, and IV can be considered as a high-energy transition-state. Finally, the $z^{\bullet}$ ions undergo facile dissociation (V – VI) into an even-electron w ion and an uncharged radical fragment that is stabilized by its allylic character and extended conjugation (VI).

Increasing the net charge of the 22 nt RNA precursor ions from 10− to 13− results in a change in EDD fragmentation pattern (Figure S3a), but the trend of increasing fragmentation next to nucleobases with decreasing IE is still evident (Figure S3b). The differences in fragmentation pattern for different precursor ion charge states (10− and 13−) could result from differences in intramolecular charge distribution. However, for EDD of $(M - 13H)^{13-}$ ions of 22 nt RNA, only ~66% of the d and w fragment ions are from cleavage next to A and G, compared to ~87% for the $(M - 10H)^{10-}$ ions. As a possible rationale, the increased Coulombic repulsion as a result of higher negative net charge of the precursor ions makes electron detachment energetically more favorable, thereby lowering the IEs and reducing the effect of nucleobase on fragmentation. Increasing the precursor ion charge from 10− to 13− has little effect on fragment ion yield; EDD of $(M - 13H)^{13-}$ ions gave 28% ions from backbone cleavage, compared to 25% in EDD of $(M - 10H)^{10-}$. Intramolecular noncovalent bonding that prevents separation of backbone fragment ions has been suggested as a reason for the low fragment ion yield in EDD of $(M - 4H)^{4-}$ ions of 15 nt DNA (0.27 charges/nt) [36]. However, our highly charged $(M - 10H)^{10-}$ and $(M - 13H)^{13-}$ 22 nt RNA ions (0.45 and 0.59 charges/nt) very likely have extended structures [50], for which fragment ion separation should not be a limiting factor.

Increasing the electron energy to 24 eV in EDD of $(M - 13H)^{13-}$ ions of 22 nt RNA gives essentially the same fragmentation pattern and dependence of yield on nucleobase IE as with 18 eV (Figure S3), but the yield of fragment ions from backbone cleavage increases to 39%. Significantly, a considerable number (9 out of 65) of higher mass fragment ions (ranging from d_{10} to w_{20}) show isotopic profiles with contributions 1 Da lower than the calculated profiles (Figure S4a). This finding indicates secondary EDD from molecular ions that have already lost an electron by electron detachment, i.e., $(M - 13H)^{12-\bullet}$ ions, and is consistent with extended ion

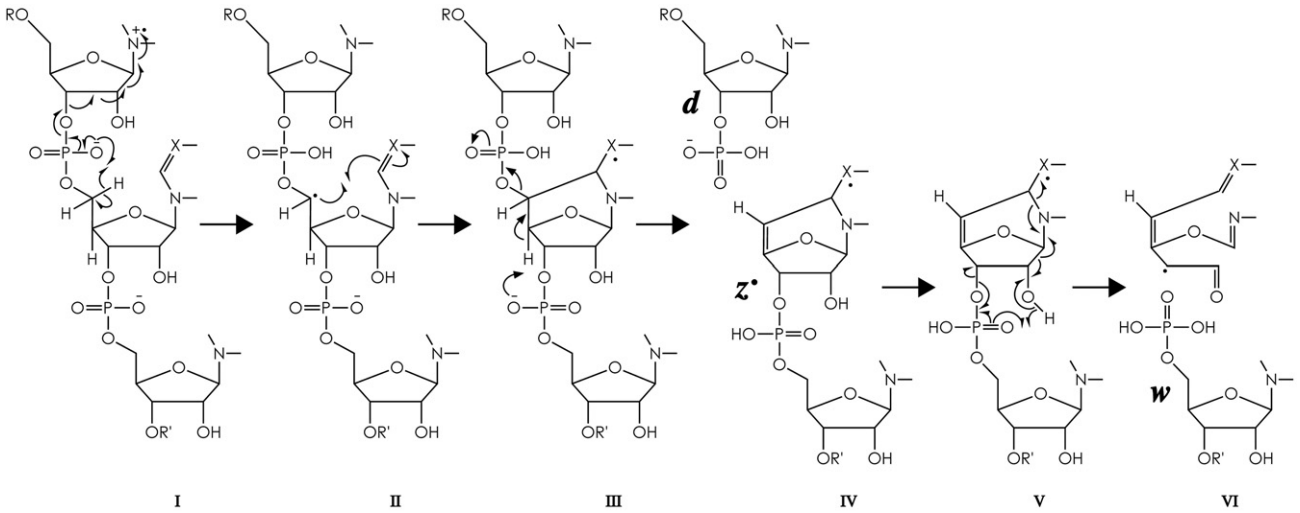

Scheme 2. Proposed mechanism for the formation of ***d*** and ***w*** ions in EDD of RNA; X stands for N (adenine, guanine) or CH (cytosine, uracil).

structures. Rather than noncovalent bonding preventing separation of fragment ions from backbone cleavage in these highly charged ions, the data suggest that structures I, II, and/or III in Scheme 2 are sufficiently stable to limit backbone dissociation in EDD. In particular, our proposed mechanism requires that the two adjacent phosphates on the 3′ side of the oxidized nucleobase are negatively charged (Scheme 2, I–III), but the probability for this is only 21% (10/21*9/20) and 37% (13/21*12/20) in the $(M - 10H)^{10-}$ and $(M - 13H)^{13-}$ ions of 22 nt RNA, respectively. Possibly "supercharging" [57, 58] of RNA $(M - nH)^{n-}$ ions could further increase EDD fragment ion yields; we are currently investigating ESI solution additives for increasing the net charge of RNA anions.

For EDD of 22 nt RNA, the yield of fragment ions is highest with higher electron energy (24 eV) and higher precursor ion charge (13−); increasing the net charge from 10− (0.45 charges/nt) to 13− (0.59 charges/nt) also effects less selective fragmentation with respect to nucleobase IE. The corresponding EDD spectrum of 22 nt RNA provides complete sequence coverage from *d* and *w* fragment ions (Figure S4b). EDD of $(M - 17H)^{17-}$ ions of 34 nt RNA (0.50 charges/nt) using 24 eV electron energy gave the spectrum in Figure 5a. With *d* and *w* fragment ions from cleavage at 32 out of 33 possible

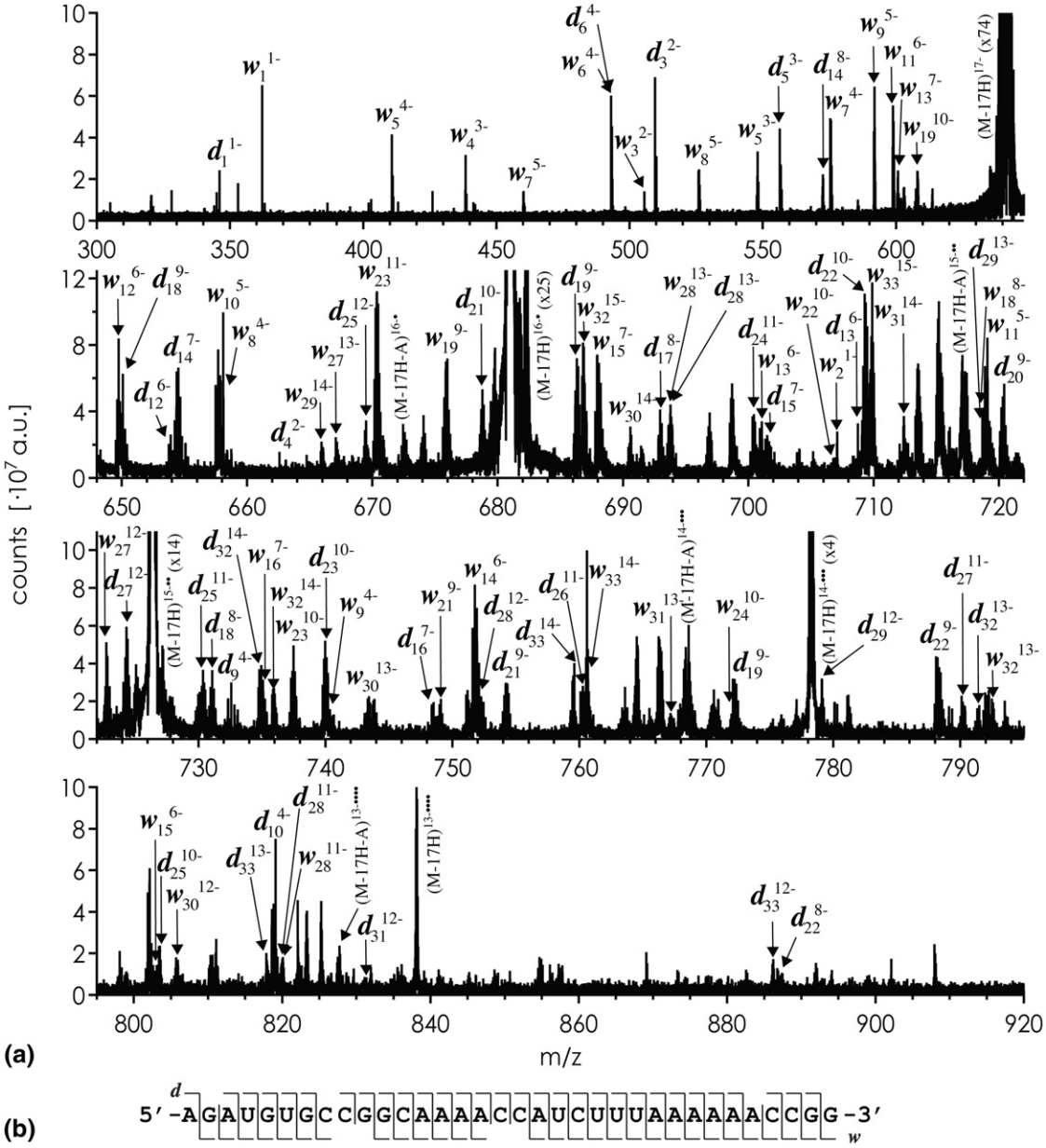

Figure 5. (**a**) EDD (electron energy 24 eV) spectrum of $(M - 17H)^{17-}$ ions from ESI of 34 nt RNA (sequence B, 1 μM in H_2O/CH_3OH 1:1, 1% vol. Et_3N, pH 9.5); (**b**) fragment ion map illustrating sequence coverage from *d* and *w* ions.

sites, sequence coverage is nearly complete (Figure 5b). Moreover, a relatively high number of "quasi-complementary" d/w ion pairs, whose mass values add up to the molecular mass plus 97.98 Da for H_3PO_4, was found: 27 out of 33 possible.

Using the same electron energy (24 eV) and a similar precursor ion charge level (0.49 charges/nt) in EDD of 61 nt RNA gave the spectrum in Figure 6a. Sequence coverage is 40%, with d and w fragment ions from cleavage at 24 out of 60 possible sites (Figure 6b). Only 6 out of 60 possible "quasi-complementary" d/w ion pairs were found. Interestingly, these are from cleavage in the U-rich 3′ terminal region; apparently the correlation of fragment ion yield with nucleobase IE (U: 9.4 eV) is masked by other factors such as higher order structure in EDD of RNA as large as 61 nt.

Conclusions

CAD of multiply deprotonated RNA gives spectra suitable for de novo sequencing when precursor ion charge is low (~0.2 charges/nt). These spectra are characterized by backbone dissociation via almost exclusively the c/y channel, minimal base loss, and reduced secondary fragmentation. RNA ions of low precursor charge can be electrosprayed from solutions with a final concentration of 25 mM piperidine/25 mM imidazole. We demonstrate here that nearly full sequence coverage (fragment ions from cleavage at 59 out of 60 possible sites) and a large number of complementary ion pairs (47 out of 59 possible) can be obtained in CAD of 61 nt RNA. The downside of using low precursor ion charge is that instrument performance, in particular sensitivity and mass resolving power, generally decrease with decreasing charge.

EDD of multiply deprotonated RNA gives spectra suitable for de novo sequencing when precursor ion charge is high (~0.5 charges/nt). For 22 nt RNA, the spectra are characterized by backbone fragmentation into exclusively d and w ions, minimal base loss, and no apparent secondary fragmentation. RNA ions of higher precursor charge can be electrosprayed from solutions with 1% vol. triethylamine added. In contrast to c and y ions, d and w ions are noncomplementary, which can be a (solvable) problem for de novo sequencing algorithms. A serious limitation in EDD, however, is the relatively low fragment ion yield (up to 39% for 22 nt RNA). Internal fragmentation also appears to be an issue in EDD of larger RNA as evidenced from the many missing "quasi-complementary" ions in the spectrum of 61 nt RNA. Moreover, fragment ion isotopic profiles can be distorted by contributions from EDD of oxidized molecular ions, making ion assignments more ambiguous. Nevertheless, we were able to demonstrate nearly complete sequence coverage along with 27 out of 33 possible "quasi-complementary" ion pairs for 34 nt RNA, and 40% sequence coverage for 61 nt RNA.

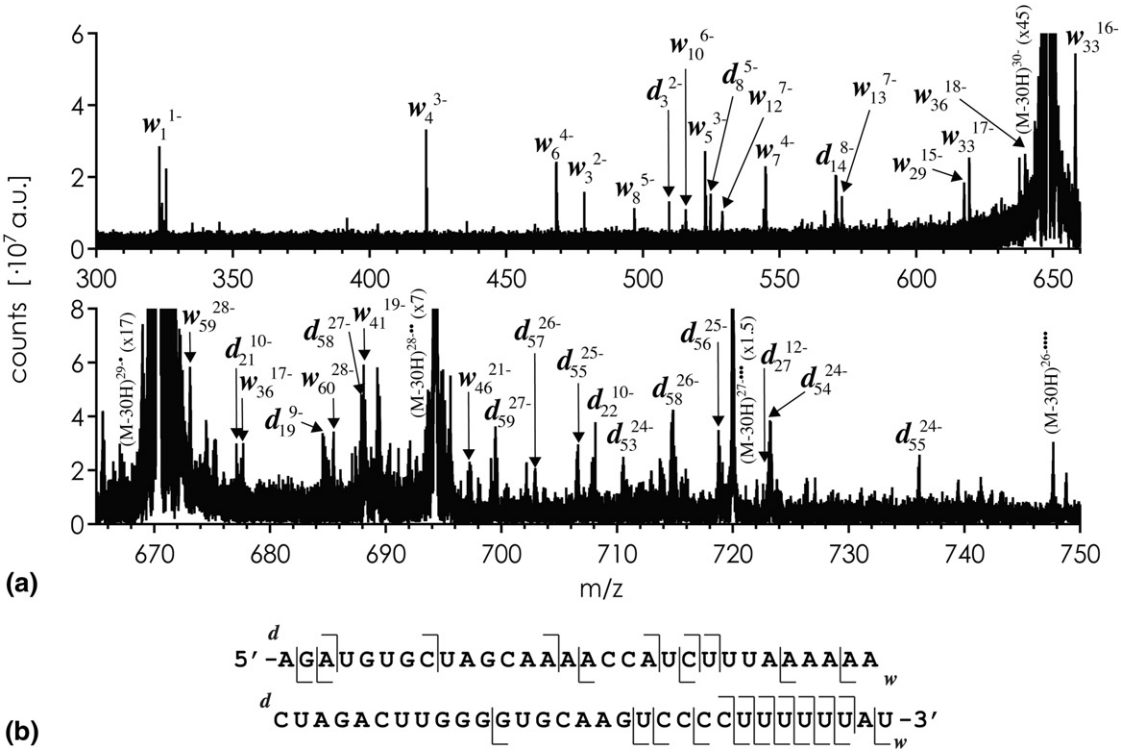

Figure 6. (**a**) EDD (electron energy 24 eV) spectrum of $(M - 30H)^{30-}$ ions from ESI of 61 nt RNA (1 μM in H_2O/CH_3OH 1:1, 1% vol. Et_3N, pH 9.5); (**b**) fragment ion map illustrating sequence coverage from d and w ions.

However, we are only beginning to understand the mechanisms of backbone dissociation in CAD and EDD of RNA; at this stage, more insights from experiment are needed to assess their full potential for top-down sequencing of even larger RNA.

Acknowledgments

The authors thank Michaela Aigner, Ulrike Rieder, and Ronald Micura (R.M.), for discussion and providing the oligonucleotide samples, and Karl Grubmayr for pointing out Bredt's rule. The authors acknowledge the Austrian Science Fund for financial support (FWF projects Y372 to K.B. and I317 to R.M.).

Appendix A Supplementary Material

Supplementary material associated with this article may be found in the online version at doi:10.1016/j.jasms.2010.02.025.

References

1. Kelleher, N. L.; Lin, H. Y.; Valaskovic, G. A.; Aaserud, D. J.; Fridriksson, E. K.; McLafferty, F. W. Top Down Versus Bottom Up Protein Characterization by Tandem High-Resolution Mass Spectrometry. *J. Am. Chem. Soc.* **1999,** *121,* 806–812.
2. Reid, G. E.; McLuckey, S. A. 'Top Down' Protein Characterization Via Tandem Mass Spectrometry. *J. Mass Spectrom.* **2002,** *37,* 663–675.
3. Han, X. M.; Jin, M.; Breuker, K.; McLafferty, F. W. Extending Top-Down Mass Spectrometry to Proteins with Masses Greater than 200 Kilodaltons. *Science* **2006,** *314,* 109–112.
4. McLafferty, F. W.; Breuker, K.; Jin, M.; Han, X. M.; Infusini, G.; Jiang, H.; Kong, X. G.; Begley, T. P. Top-Down MS, a Powerful Complement to the High Capabilities of Proteolysis Proteomics. *FEBS J.* **2007,** *274,* 6256–6268.
5. Breuker, K.; Jin, M.; Han, X. M.; Jiang, H. H.; McLafferty, F. W. Top-Down Identification and Characterization of Biomolecules by Mass Spectrometry. *J. Am. Soc. Mass Spectrom.* **2008,** *19,* 1045–1053.
6. McLafferty, F. W.; Bente, P. F.; Kornfeld, R.; Tsai, S. C.; Howe, I. Collisional Activation Spectra of Organic Ions. *J. Am. Chem. Soc.* **1973,** *95,* 2120–2129.
7. Laskin, J.; Futrell, J. H. Activation of Large Ions in FT-ICR Mass Spectrometry. *Mass Spectrom. Rev.* **2005,** *24,* 135–167.
8. Laskin, J.; Futrell, J. H. Collisional Activation of Peptide Ions in FT-ICR Mass Spectrometry. *Mass Spectrom. Rev.* **2003,** *22,* 158–181.
9. Zubarev, R. A.; Kelleher, N. L.; McLafferty, F. W. Electron Capture Dissociation of Multiply Charged Protein Cations. A Nonergodic Process. *J. Am. Chem. Soc.* **1998,** *120,* 3265–3266.
10. Cooper, H. J.; Håkansson, K.; Marshall, A. G. The Role of Electron Capture Dissociation in Biomolecular Analysis. *Mass Spectrom. Rev.* **2005,** *24,* 201–222.
11. Horn, D. M.; Ge, Y.; McLafferty, F. W. Activated Ion Electron Capture Dissociation for Mass Spectral Sequencing of Larger (42 kDa) Proteins. *Anal. Chem.* **2000,** *72,* 4778–4784.
12. Breuker, K.; Oh, H. B.; Horn, D. M.; Cerda, B. A.; McLafferty, F. W. Detailed Unfolding and Folding of Gaseous Ubiquitin Ions Characterized by Electron Capture Dissociation. *J. Am. Chem. Soc.* **2002,** *124,* 6407–6420.
13. Syka, J. E. P.; Coon, J. J.; Schroeder, M. J.; Shabanowitz, J.; Hunt, D. F. Peptide and Protein Sequence Analysis by Electron Transfer Dissociation Mass Spectrometry. *Proc. Natl. Acad. Sci. U.S.A.* **2004,** *101,* 9528–9533.
14. McLuckey, S. A.; Vanberkel, G. J.; Glish, G. L. Tandem Mass-Spectrometry of Small, Multiply Charged Oligonucleotides. *J. Am. Soc. Mass Spectrom.* **1992,** *3,* 60–70.
15. McLuckey, S. A. Habibigoudarzi, S. Decompositions of Multiply-Charged Oligonucleotide Anions. *J. Am. Chem. Soc.* **1993,** *115,* 12085–12095.
16. Little, D. P.; Chorush, R. A.; Speir, J. P.; Senko, M. W.; Kelleher, N. L.; McLafferty, F. W. Rapid Sequencing of Oligonucleotides by High-Resolution Mass-Spectrometry. *J. Am. Chem. Soc.* **1994,** *116,* 4893–4897.
17. Little, D. P.; Aaserud, D. J.; Valaskovic, G. A.; McLafferty, F. W. Sequence Information from 42-108-mer DNAs (Complete for a 50-mer) by Tandem Mass Spectrometry. *J. Am. Chem. Soc.* **1996,** *118,* 9352–9359.
18. Wu, J.; McLuckey, S. A. Gas-Phase Fragmentation of Oligonucleotide Ions. *Int. J. Mass Spectrom.* **2004,** *237,* 197–241.
19. Hüttenhofer, A.; Schattner, P.; Polacek, N. Non-Coding RNAs: Hope or Hype? *Trends Genet.* **2005,** *21,* 289–297.
20. Kellersberger, K. A.; Yu, E.; Kruppa, G. H.; Young, M. M.; Fabris, D. Top-Down Characterization of Nucleic Acids Modified by Structural Probes Using High-Resolution Tandem Mass Spectrometry and Automated Data Interpretation. *Anal. Chem.* **2004,** *76,* 2438–2445.
21. Turner, K. B.; Hagan, N. A.; Kohlway, A. S.; Fabris, D. Mapping Noncovalent Ligand Binding to Stemloop Domains of the HIV-1 Packaging Signal by Tandem Mass Spectrometry. *J. Am. Soc. Mass Spectrom.* **2006,** *17,* 1401–1411.
22. Keller, K. M.; Breeden, M. M.; Zhang, J. M.; Ellington, A. D.; Brodbelt, J. S. Electrospray Ionization of Nucleic Acid Aptamer/Small Molecule Complexes for Screening Aptamer Selectivity. *J. Mass Spectrom.* **2005,** *40,* 1327–1337.
23. Griffey, R. H.; Hofstadler, S. A.; Sannes-Lowery, K. A.; Ecker, D. J.; Crooke, S. T. Determinants of Aminoglycoside-Binding Specificity for rRNA by Using Mass Spectrometry. *Proc. Natl. Acad. Sci. U.S.A.* **1999,** *96,* 10129–10133.
24. Fenn, J. B.; Mann, M.; Meng, C. K.; Wong, S. F.; Whitehouse, C. M. Electrospray Ionization for Mass Spectrometry of Large Biomolecules. *Science* **1989,** *246,* 64–71.
25. Huang, T. Y.; Liu, J.; Liang, X. R.; Hodges, B. D. M.; McLuckey, S. A. Collision-Induced Dissociation of Intact Duplex and Single-Stranded siRNA Anions. *Anal. Chem.* **2008,** *80,* 8501–8508.
26. Taucher, M.; Rieder, U.; Breuker, K. Minimizing Base Loss and Internal Fragmentation in Collisionally Activated Dissociation of Multiply Deprotonated RNA. *J. Am. Soc. Mass Spectrom.* **2010,** *21,* 278–285.
27. Huang, T. Y.; Kharlamova, A.; Liu, J.; McLuckey, S. A. Ion Trap Collision-Induced Dissociation of Multiply Deprotonated RNA: *c*/*y*-Ions Versus (*a*-B)/*w*-Ions. *J. Am. Soc. Mass Spectrom.* **2008,** *19,* 1832–1840.
28. Wolff, J. J.; Laremore, T. N.; Busch, A. M.; Linhardt, R. J.; Amster, I. J. Influence of Charge State and Sodium Cationization on the Electron Detachment Dissociation and Infrared Multiphoton Dissociation of Glycosaminoglycan Oligosaccharides. *J. Am. Soc. Mass Spectrom.* **2008,** *19,* 790–798.
29. Yang, J.; Håkansson, K. Characterization and Optimization of Electron Detachment Dissociation Fourier Transform Ion Cyclotron Resonance Mass Spectrometry. *Int. J. Mass Spectrom.* **2008,** *276,* 144–148.
30. Budnik, B. A.; Haselmann, K. F.; Zubarev, R. A. Electron Detachment Dissociation of Peptide Di-Anions: An Electron-Hole Recombination Phenomenon. *Chem. Phys. Lett.* **2001,** *342,* 299–302.
31. Kjeldsen, F.; Silivra, O. A.; Ivonin, I. A.; Haselmann, K. F.; Gorshkov, M.; Zubarev, R. A. C.-&;α-C Backbone Fragmentation Dominates in Electron Detachment Dissociation of Gas-Phase Polypeptide Polyanions. *Chem. A Eur. J.* **2005,** *11,* 1803–1812.
32. Liu, H.; Håkansson, K. Electron Capture Dissociation of Tyrosine O-Sulfated Peptides Complexed with Divalent Metal Cations. *Anal. Chem.* **2006,** *78,* 7570–7576.
33. Kjeldsen, F.; Horning, O. B.; Jensen, S. S.; Giessing, A. M. B.; Jensen, O. N. Towards Liquid Chromatography Time-Scale Peptide Sequencing and Characterization of Post-Translational Modifications in the Negative-Ion Mode Using Electron Detachment Dissociation Tandem Mass Spectrometry. *J. Am. Soc. Mass Spectrom.* **2008,** *19,* 1156–1162.
34. Yang, J.; Mo, J. J.; Adamson, J. T.; Håkansson, K. Characterization of Oligodeoxynucleotides by Electron Detachment Dissociation Fourier Transform Ion Cyclotron Resonance Mass Spectrometry. *Anal. Chem.* **2005,** *77,* 1876–1882.
35. Yang, J.; Håkansson, K. Fragmentation of Oligoribonucleotides from Gas-Phase Ion-Electron Reactions. *J. Am. Soc. Mass Spectrom.* **2006,** *17,* 1369–1375.
36. Mo, J. J.; Håkansson, K. Characterization of Nucleic Acid Higher Order Structure by High-Resolution Tandem Mass Spectrometry. *Anal. Bioanal. Chem.* **2006,** *386,* 675–681.
37. Kinet, C.; Gabelica, V.; Balbeur, D.; De Pauw, E. Electron Detachment Dissociation (EDD) Pathways in Oligonucleotides. *Int. J. Mass Spectrom.* **2009,** *283,* 206–213.
38. Yang, J.; Håkansson, K. Characterization of Oligodeoxynucleotide Fragmentation Pathways in Infrared Multiphoton Dissociation and Electron Detachment Dissociation by Fourier Transform Ion Cyclotron Double Resonance. *Eur. J. Mass Spectrom.* **2009,** *15,* 293–304.
39. Wolff, J. J.; Amster, I. J.; Chi, L. L.; Linhardt, R. J. Electron Detachment Dissociation of Glycosaminoglycan Tetrasaccharides. *J. Am. Soc. Mass Spectrom.* **2007,** *18,* 234–244.
40. Wolff, J. J.; Chi, L. L.; Linhardt, R. J.; Amster, I. J. Distinguishing Glucuronic from Iduronic Acid in Glycosaminoglycan Tetrasaccharides by Using Electron Detachment Dissociation. *Anal. Chem.* **2007,** *79,* 2015–2022.
41. Leach, F. E.; Wolff, J. J.; Laremore, T. N.; Linhardt, R. J.; Amster, I. J. Evaluation of the Experimental Parameters Which Control Electron Detachment Dissociation, and Their Effect on the Fragmentation Efficiency of Glycosaminoglycan Carbohydrates. *Int. J. Mass Spectrom.* **2008,** *276,* 110–115.
42. Wolff, J. J.; Laremore, T. N.; Aslam, H.; Linhardt, R. J.; Amster, I. J. Electron-Induced Dissociation of Glycosaminoglycan Tetrasaccharides. *J. Am. Soc. Mass Spectrom.* **2008,** *19,* 1449–1458.
43. Wolff, J. J.; Laremore, T. N.; Busch, A. M.; Linhardt, R. J.; Amster, I. J. Electron Detachment Dissociation of Dermatan Sulfate Oligosaccharides. *J. Am. Soc. Mass Spectrom.* **2008,** *19,* 294–304.
44. Yang, J. Håkansson, K. Fragmentation of Oligoribonucleotides from Gas-Phase Ion-Electron Reactions. *J. Am. Soc. Mass Spectrom.* **2006,** *17,* 1369–1375.

45. Micura, R. Small Interfering RNAs and Their Chemical Synthesis. *Angew. Chem. Int. Ed.* **2002,** *41,* 2265–2269.
46. Greig, M.; Griffey, R. H. Utility of Organic-Bases for Improved Electrospray Mass-Spectrometry of Oligonucleotides. *Rapid Commun. Mass Spectrom.* **1995,** *9,* 97–102.
47. Schnier, P. D.; Gross, D. S.; Williams, E. R. On the Maximum Charge-State and Proton-Transfer Reactivity of Peptide and Protein Ions Formed by Electrospray-Ionization. *J. Am. Soc. Mass Spectrom.* **1995,** *6,* 1086–1097.
48. Iavarone, A. T.; Williams, E. R. Mechanism of Charging and Supercharging Molecules in Electrospray Ionization. *J. Am. Chem. Soc.* **2003,** *125,* 2319–2327.
49. Marshall, A. G.; Hendrickson, C. L. Charge Reduction Lowers Mass Resolving Power for Isotopically Resolved Electrospray Ionization Fourier Transform Ion Cyclotron Resonance Mass Spectra. *Rapid Commun. Mass Spectrom.* **2001,** *15,* 232–235.
50. Moradian, A.; Scalf, M.; Westphall, M. S.; Smith, L. M.; Douglas, D. J. Collision Cross Sections of Gas Phase DNA Ions. *Int. J. Mass Spectrom.* **2002,** *219,* 161–170.
51. Verkin, B. I.; Sukhodub, L. F.; Yanson, I. K. Potentials of Ionization of Nitrogen Bases of Nucleic-Acids. *Doklady Akademii Nauk SSSR* **1976,** *228,* 1452–1455.
52. Galenica, V.; Tabarin, T.; Antoine, R.; Rosu, F.; Compagnon, I.; Broyer, M.; De Pauw, E.; Dugourd, P. Electron Photodetachment Dissociation of DNA Polyanions in a Quadrupole Ion Trap Mass Spectrometer. *Anal. Chem.* **2006,** *78,* 6564–6572.
53. Randerath, K.; Zhou, G. D.; Somers, R. L.; Robbins, J. H.; Brooks, P. J. A P-32-Postlabeling Assay for the Oxidative DNA Lesion 8,5′-Cyclo-2′-Deoxyadenosine in Mammalian Tissues—Evidence That Four Type II I-Compounds are Dinucleotides Containing the Lesion in the 3′ Nucleotide. *J. Biol. Chem.* **2001,** *276,* 36051–36057.
54. Dizdaroglu, M.; Jaruga, P.; Rodriguez, H. Identification and Quantification of 8,5′-Cyclo-2′-Deoxyadenosine in DNA by Liquid Chromatography/Mass Spectrometry. *Free Rad. Biol. Med.* **2001,** *30,* 774–784.
55. Jaruga, P.; Birincioglu, M.; Rodriguez, H.; Dizdaroglu, M. Mass Spectrometric Assays for the Tandem Lesion 8,5′-Cyclo-2′-Deoxyguanosine in Mammalian DNA. *Biochemistry* **2002,** *41,* 3703–3711.
56. Zhang, R. B.; Eriksson, L. A. Theoretical Study of the Tandem Cross-Linkage Lesion in DNA. *Chem. Phys. Lett.* **2006,** *417,* 303–308.
57. Iavarone, A. T.; Williams, E. R. Supercharging in Electrospray Ionization: Effects on Signal and Charge. *Int. J. Mass Spectrom.* **2002,** *219,* 63–72.
58. Iavarone, A. T.; Williams, E. R. Mechanism of Charging and Supercharging Molecules in Electrospray Ionization. *J. Am. Chem. Soc.* **2003,** *125,* 2319–2327.